Modeling and analysis of composite wing sections for improved aeroelastic and vibration characteristics using smart materials

Grant Number NAG-1-1648
Period of Performance: Jan. 1 - Sept. 30, 1996
PI - Aditi Chattopadhyay
Graduate Research Assistant - Charles E. Seeley
Technical monitor - Anna McGowan
Arizona State University
Department of Mechanical and Aerospace Engineering
Tempe, Arizona 85287

October 4, 1996

Modeling and analysis of composite wing sections for improved aeroelastic and vibration characteristics using smart materials

PI - Aditi Chattopadhyay
Graduate Research Assistant - Charles E. Seeley
Arizona State University
Department of Mechanical and Aerospace Engineering
Tempe, Arizona 85287

Objectives

The objective of this research is to develop analysis procedures to investigate the coupling of composite and smart materials to improve aeroelastic and vibratory response of aerospace structures. The structural modeling must account for arbitrarily thick geometries, embedded and surface bonded sensors and actuators and imperfections, such as delamination. Changes in the dynamic response due to the presence of smart materials and delaminations is investigated. Experiments are to be performed to validate the proposed mathematical model.

Introduction

Laminated composite structural elements with surface bonded/embedded sensors and actuators offer great potential for static and dynamic control. Essential to designing these advanced structures are accurate and efficient mathematical modeling techniques. Imperfections, such as delaminations, are common to most composites and must be included in the analysis procedure. Several mathematical models have appeared in the literature for the analysis of adaptive beams and plates. These include investigations based on the classical theory [1,2], which is limited to the analysis of thin plates, first order Mindlin type analyses [3,4] and potentially expensive layer-wise theories [5,6]. A hybrid theory has also been presented by Mitchel and Reddy [7]. Higher order refined theory is both accurate and computationally efficient and have been shown to be useful for modeling smart composite laminates [8,9]. Finite element models [3,5,9] are attractive since they can include practical geometries and boundary conditions.

---

* Graduate Research Assistant, Student Member AIAA, ASME
† Associate Professor, Associate Fellow AIAA, Member SPIE, ASME, AHS, ISSMO, AAM

Several efforts for modeling delamination of composite laminates have been presented in the literature. Although three dimensional approaches [10,11] are more accurate than two dimensional theories [12-15], their implementation can be very expensive for practical applications. The layer-wise approach [16] is an alternative since it is capable of modeling displacement discontinuities. However, the computational effort increases with the number of plies. Recently, a refined higher order theory, developed by Gu and Chattopadhyay [17], was shown to be an efficient approach for modeling delaminations. This theory has been shown to agree well with both elasticity solutions [18] and experimental results [17].

Relatively little attention in the literature has been paid to modeling delaminated smart composites with surface bonded/embedded piezoelectric actuators and sensors [19,20]. Therefore, the goal of the current work is to investigate this important topic. The refined higher order theory is used. This theory allows for transverse shear deformation which is especially important in the analysis of composites thick composites. It also allows for both slipping and separation of the delaminated regions. The finite element implementation allows practical geometries and boundary conditions to be modeled as well.

Analysis

In the developed theory, the composite laminate is divided into several regions which represent the nondelaminated zone and portions of the composite laminate above and below the delamination. The refined theory is implemented in each region by satisfying the stress free boundary conditions which occur at the top and bottom surfaces of the laminate as well as at the delamination interface. This allows several of the higher order functions to be determined in terms of the lower order functions. Continuity conditions are formulated between the regions. These conditions are enforced in the finite element implementation using a penalty approach. The theory can be easily generalized to include multiple piezoelectric sensors, actuators and delaminations as shown in Fig. 1.

The general displacement field with parameters indicated in Fig. 2 is defined as follows.

$$U(x,y,z) = u(x,y) + (z-c)\left(-\frac{\partial}{\partial x}w(x,y) + \phi_x(x,y)\right) + (z-c)^2 u_2(x,y) + (z-c)^3 u_3(x,y)$$
$$V(x,y,z) = v(x,y) + (z-c)\left(-\frac{\partial}{\partial y}w(x,y) + \phi_y(x,y)\right) + (z-c)^2 v_2(x,y) + (z-c)^3 v_3(x,y) \quad (1)$$
$$W(x,y,z) = w(x,y)$$

where U, V and W are the total displacements, u, v and w denote the midplane displacements of a point (x,y), the partial derivatives of w represent the rotations of normals to the midplane corresponding to the slope of the laminate and ϕ_x and ϕ_y represent the additional rotations due to shear deformation about the y and x axes, respectively. The quantities u_2, u_3, v_2 and v_3 represent higher order functions. This displacement field has the advantage of easily reducing to the well known classical theory if the higher order terms are eliminated. The thickness coordinate, z, is measured from the global midplane of the laminate and c is the local midplane where c = 0 for an undelaminated composite.

Constitutive relations

Equations which relate stress, strain, charge and electric field are derived from the electric enthalpy density function given as follows.

$$H(\varepsilon_{ij}, E_i) = \frac{1}{2}c_{ijkl}\varepsilon_{ij}\varepsilon_{kl} - e_{ijk}E_i\varepsilon_{jk} - \frac{1}{2}k_{ij}E_iE_j \quad (2)$$

where ε_{ij} and E_i are components of the strain tensor and electric field vector, respectively and c_{ijkl}, e_{ijk}, and k_{ij} are the elastic, piezoelectric and dielectric permittivity constants, respectively. The stress and charge are determined as follows.

$$D_i = -\frac{\partial H}{\partial E_i} \quad (3)$$

$$\sigma_{ij} = \frac{\partial H}{\partial \varepsilon_{ij}} \quad (4)$$

For an orthotropic composite laminate with piezoelectric layers that have orthorhombic mm2 symmetry in the context of laminate theory, the constitutive relationships are simplified as follows.

$$\begin{bmatrix}\sigma_1\\ \sigma_2\\ \sigma_3\\ \sigma_4\\ \sigma_5\\ \sigma_6\end{bmatrix}_k = \begin{bmatrix}\overline{Q}_{11} & \overline{Q}_{12} & 0 & 0 & 0 & \overline{Q}_{16}\\ \overline{Q}_{12} & \overline{Q}_{22} & 0 & 0 & 0 & \overline{Q}_{26}\\ 0 & 0 & 0 & 0 & 0 & 0\\ 0 & 0 & 0 & \overline{Q}_{44} & \overline{Q}_{45} & 0\\ 0 & 0 & 0 & \overline{Q}_{45} & \overline{Q}_{55} & 0\\ \overline{Q}_{16} & \overline{Q}_{26} & 0 & 0 & 0 & \overline{Q}_{66}\end{bmatrix}_k \begin{bmatrix}\varepsilon_1 - \Lambda_1\\ \varepsilon_2 - \Lambda_2\\ \varepsilon_3\\ \varepsilon_4\\ \varepsilon_5\\ \varepsilon_6\end{bmatrix}_k \tag{5}$$

$$D_{3_k} = \begin{bmatrix}d_{31} & d_{32}\end{bmatrix}_k \begin{bmatrix}\overline{Q}_{11} & \overline{Q}_{21}\\ \overline{Q}_{21} & \overline{Q}_{22}\end{bmatrix}_k \begin{bmatrix}\varepsilon_1\\ \varepsilon_2\end{bmatrix}_k \tag{6}$$

where Λ are the induced strains ($\Lambda_1 = \Lambda_2 = d_{31}E_3$). It is important to note that engineering normal ($\varepsilon_{1\text{-}3}$) and shear ($\varepsilon_{4\text{-}6}$) strains are now used in the above equations, ε_3 is set to zero and only the inplane piezoelectric constants (d_{31} and d_{32}) are retained in the context of the current work.

Refined displacement field

To account for the effects due to delamination, it is necessary to partition the laminate into several different regions shown in Fig. 3. These regions include the nondelaminated region (Ω), the region above the delamination (Ω_{d2}) and the region below the delamination (Ω_{d3}). The interface between the nondelaminated region and the delaminated regions, indicated by the dashed line in Fig. 3, is denoted Ω_I. The general form of the higher order displacement field (Eqn. 1) is independently applied to each of these regions to describe displacements which account for slipping and separation due to the delamination. However, this displacement field does not necessarily satisfy the condition that the transverse shear stresses, σ_4 and σ_5, vanish at the top and bottom surfaces of the plate ($z = \pm h/2$) as well as on the debonded interface surfaces ($z = h_1$)in the delaminated region. That is,

$$\sigma_4(x,y,\pm h/2) = 0, \quad \sigma_5(x,y,\pm h/2) = 0 \tag{7}$$

$$\sigma_4(x,y,h_1) = 0, \quad \sigma_5(x,y,h_1) = 0 \quad (x,y) \in \Omega_d \tag{8}$$

in which the superscripts "+" and "-" denote the quantities related to the layers above and below the delamination, respectively, and Ω_d refers to the region that contains the delamination. For orthotropic plates, these conditions are equivalent to the requirement that the corresponding strains

be zero on these surfaces. A refined displacement field is obtained by applying these boundary conditions for each region as follows.

$$U_{1_i} = u_i + (z - c_i)\left(-\frac{\partial w_i}{\partial x} + \phi_{x_i}\right) - (z - c_i)^3 \frac{4}{3{d_i}^2}\phi_{x_i}$$

$$U_{2_i} = v_i + (z - c_i)\left(-\frac{\partial w_i}{\partial y} + \phi_{y_i}\right) - (z - c_i)^3 \frac{4}{3{d_i}^2}\phi_{y_i} \quad (i = 1,2,3) \tag{9}$$

$$U_{3_i} = w_i$$

where $c_i = \frac{(a_i + b_i)}{2}$ is the local midplane and $d_i = b_i - a_i$ is the thickness of the region. The quantities a_i and b_i correspond to the bottom and top coordinates of the local region, respectively, as shown in Fig. 4. It is important to note that several of the higher order terms in the generalized displacement field are either found to be zero or defined in terms of lower order functions. The displacements in each region are defined by independent functions with parameters given as follows.

$$\text{when} \quad i = 1 \quad \begin{Bmatrix} a_i \\ b_i \end{Bmatrix} = \begin{Bmatrix} h/2 \\ -h/2 \end{Bmatrix}, \quad (x,y) \in \Omega \tag{10a}$$

$$\text{when} \quad i = 2 \quad \begin{Bmatrix} a_i \\ b_i \end{Bmatrix} = \begin{Bmatrix} h/2 \\ h_1 \end{Bmatrix}, \quad (x,y) \in \Omega_{d2} \tag{10b}$$

$$\text{when} \quad i = 3 \quad \begin{Bmatrix} a_i \\ b_i \end{Bmatrix} = \begin{Bmatrix} h_1 \\ -h/2 \end{Bmatrix}, \quad (x,y) \in \Omega_{d3} \tag{10c}$$

It is important to note that the thickness of the plate, h, may vary due to the presence of surface bonded sensors/actuators.

Continuity Conditions

Additional boundary conditions must be imposed to ensure continuity of displacements at the interface of the nondelaminated and delaminated regions (Ω_I) as shown in Fig. 5. A vector of the displacements is constructed to simplify formulation of the boundary conditions as follows.

$$U_i = \begin{bmatrix} U_i \\ V_i \\ W_i \end{bmatrix} \tag{11}$$

The continuity conditions at the interface of the nondelaminated and delaminated regions (Ω_I), are imposed as follows.

$$U_{i=1} = U_{i=2} \quad a_2 < z \le \min(b_1, b_2) \qquad (x,y) \in \Omega_I \tag{12}$$

$$U_{i=1} = U_{i=3} \quad \max(a_1, a_2) < z \le b_3 \qquad (x,y) \in \Omega_I \tag{13}$$

The above equations can be satisfied exactly for the classical theory since the displacement distribution through the thickness is linear. However, the displacement distribution using the refined theory is nonlinear and must be satisfied in an average sense as follows. An error function vector for the first of the above equations is formulated as follows.

$$e = U_{i=1} - U_{i=2} \quad h1 < z \le h/2 \qquad (x,y) \in \Omega_I \tag{14}$$

It is desired to minimize the difference between $U_{i=1}$ and $U_{i=2}$ at each point through the thickness in Ω_I. This can be accomplished by first integrating the square of the error through the thickness as follows.

$$E = \frac{1}{2}\int_a^b \left(e^T e\right) dz \tag{15}$$

where a and b define the limits of integration through the thickness as indicated in the interval given in Eqn. 13 These integration limits must be considered carefully since the presence of surface bonded actuators/sensors may change the dimensions of the laminate in any of the regions. It is desired to find a relationship between the independent functions in Ω and Ω_{dI} which minimizes the error in terms of the functions in the nondelaminated region to satisfy the continuity conditions. Therefore, derivatives of E are taken with respect to the independent functions in Ω_{dI} and are set to zero as follows.

$$\frac{\partial E}{\partial u_{i=2}} = 0, \qquad \frac{\partial E}{\partial v_{i=2}} = 0, \qquad \frac{\partial E}{\partial w_{i=2}} = 0,$$

$$\frac{\partial E}{\partial\left(\frac{\partial w_{i=2}}{\partial x}\right)} = 0, \qquad \frac{\partial E}{\partial\left(\frac{\partial w_{i=2}}{\partial y}\right)} = 0 \tag{16a-f}$$

$$\frac{\partial E}{\partial \phi_{x_{i=2}}} = 0, \qquad \frac{\partial E}{\partial \phi_{y_{i=2}}} = 0$$

Taking derivatives and rearranging the above equations leads to the following relationships which satisfy the continuity conditions.

$$u_i = u_1 + (c_1 - c_i)\frac{\partial w_1}{\partial x} + \alpha_i \phi_{x_1}$$

$$v_i = v_1 + (c_1 - c_i)\frac{\partial w_1}{\partial y} + \alpha_i \phi_{y_1}$$

$$w_i = w_1$$

$$\frac{\partial w_i}{\partial x} = \frac{\partial w_1}{\partial x} + \beta_i \phi_{x_1} \qquad (17a\text{-}g)$$

$$\frac{\partial w_i}{\partial y} = \frac{\partial w_1}{\partial y} + \beta_i \phi_{y_1}$$

$$\phi_{x_i} = \frac{\partial w_1}{\partial x} + \gamma_i \phi_{x_1}$$

$$\phi_{y_i} = \frac{\partial w_1}{\partial y} + \gamma_i \phi_{y_1}$$

where i = 2 and the above relationships correspond to Ω and Ω_{d2}, respectively. The constants α_i, β_i, and γ_i are as follows.

$$\alpha_i = (-4a^4 - 36a^3b - 60a^2b^2 - 36ab^3 - 4b^4 + 36a^2c_1^2 + 68abc_1^2 + 36b^2c_1^2 + 52a^3c_i + 228a^2bc_i + 228ab^2c_i + 52b^3c_i - 72a^2c_1c_i - 136abc_1c_i - 72b^2c_1c_i - 140ac_1^2c_i - 140bc_1^2c_i - 156a^2c_i^2 - 388abc_i^2 - 156b^2c_i^2 + 280ac_1c_i^2 + 280bc_1c_i^2 + 140c_1^2c_i^2 + 140ac_i^3 + 140bc_i^3 - 280c_1c_i^3 - 27a^2d_1^2 - 51abd_1^2 - 27b^2d_1^2 + 105ac_id_1^2 + 105bc_id_1^2 - 105c_i^2d_1^2)/(3(9a^2 + 17ab + 9b^2 - 35ac_i - 35bc_i + 35c_i^2)d_1^2 \qquad (18)$$

$$\beta_i = (18a^2 + 34ab + 18b^2 - 35ac_1 - 35bc_1 - 35ac_i - 35bc_i + 70c_1c_i)d_i^2/(2(9a^2 + 17ab + 9b^2 - 35ac_i - 35bc_i + 35c_i^2)d_1^2) \qquad (19)$$

$$\gamma_i = (-30a^3c_1 - 110a^2bc_1 - 110ab^2c_1 - 30b^3c_1 + 72a^2c_1^2 + 136abc_1^2 + 72b^2c_1^2 + 30a^3c_i + 110a^2bc_i + 110ab^2c_i + 30b^3c_i + 56a^2c_1c_i + 168abc_1c_i + 56b^2c_1c_i - 280ac_1^2c_i - 280bc_1^2c_i - 128a^2c_i^2 - 304abc_i^2 - 128b^2c_i^2 + 140ac_1c_i^2 + 140bc_1c_i^2 + 280c_1^2c_i^2 + 140ac_i^3 + 140bc_i^3 - 280c_1c_i^3 - 18a^2d_1^2 - 34abd_1^2 - 18b^2d_1^2 + 70ac_id_1^2 + 70bc_id_1^2 - 70c_i^2d_1^2 + 18a^2d_i^2 + 34abd_i^2 + 18b^2d_i^2 - 35ac_1d_i^2 - 35bc_1d_i^2 - 35ac_id_i^2 - 35bc_id_i^2 + 70c_1c_id_i^2)/(2(9a^2 + 17ab + 9b^2 - 35ac_i - 35bc_i + 35c_i^2)d_1^2) \qquad (20)$$

Identical expressions are formulated which correspond to Ω and Ω_{d3} by setting i = 3. Multiple delaminations can be incorporated into the developed theory by defining additional regions of delamination at arbitrary locations in the laminate (i.e. i = 1, 2, 3, 4, 5, 6 ...).

Finite element analysis

The finite element equations are derived using the discretized form of Hamilton's principle, which is stated as follows.

$$\delta\Pi = \int_{t_1}^{t_2} \sum_{e=1}^{N_e} \left[\delta K^e - \delta U^e + \delta W^e\right] dt = 0 \tag{21}$$

where t_1 and t_2 are the initial and the final times, respectively and δK^e, δU^e and δW^e are the element variations in the kinetic, strain and potential energies, respectively. The finite element matrices are formulated as follows.

$$\int_{t_1}^{t_2} \sum_{e=1}^{N_e} \left[\delta u^e M^e \ddot{u}^e + \delta u^e K^e u^e - \delta u^e \left(F^e + F_p^e\right)\right] = 0 \tag{22}$$

where N_e is the number of elements, an overdot indicates a derivative with respect to time and the nodal degrees of freedom for each element, u_n^e, are specified as follows.

$$u_n^e = \left[u_n \quad v_n \quad w_n \quad \frac{\partial w_n}{\partial x} \quad \frac{\partial w_n}{\partial y} \quad \phi_{x_n} \quad \phi_{y_n}\right]^T \tag{23}$$

Elemental nodes for the nondelaminated and delaminated regions are placed at the local midplanes of each region as shown in Fig. 6. The mass matrix, M^e, is formulated as follows.

$$M^e = \int_{A^e} \rho N^{eT} Z N^e dA^e \tag{24}$$

where ρ is the density, N^e contains the elemental shape functions and Z contains the z dependence of the displacement fields. The stiffness matrix, K^e, includes bending and extension terms (subscript B) and transverse shear terms (subscript T)

$$K^e = \int_{A^e} B_B^{eT} A_B B_B^e dA^e + \int_{A^e} B_T^{eT} A_T B_T^e dA^e \tag{25}$$

where A_B and A_T are laminate stiffness matrices and B_B^e and B_T^e relate the strains to the interpolated functions. The subscripts "B" and "T" correspond to the extension/bending and transverse shear strains, respectively. Two force vectors are formulated for the distributed load, F^e , and the piezoelectric forces, F_p^e .

$$F^e = \int_{A^e} N_B^{eT} p^e(x,y) dA^e \tag{26}$$

$$F_P^e = \int_{A^e} N_B^{eT} A_{B_p} \Lambda dA^e \tag{27}$$

The linear finite element equations of motion are obtained as follows.

$$M\ddot{u} + Ku = F + F_P \tag{28}$$

where the quantities **M**, **K** , **F** and **w** denote the mass and stiffness matrices, the force vector due to a distributed load and the nodal displacement vector, respectively. The quantity $\mathbf{F_P}$ is the force vector due to the piezoelectric actuation. Bilinear shape functions are used for the inplane displacements and rotations (u, v, ϕ_x, ϕ_y) while a 12 term cubic polynomial is used for the transverse displacements (w). The resulting four noded rectangular elements are nonconforming for computational efficiency and contain 28 degrees of freedom each.

Implementation of continuity conditions

The continuity conditions between the nondelaminated and delaminated regions need to be included in the finite element model by constraining the nodal degrees of freedom at the interface of the nondelaminated and the delaminated regions. Applying these constraints directly to Eqn. 28 leads to a nonsymmetric system of equations which results in undesirable consequences in the solution technique. A different approach must be used. The continuity conditions presented in Eqns. 17a-g for the regions Ω and Ω_{d2}, as well as similar conditions for the regions Ω and Ω_{d3}, are applied to the finite element degrees of freedom at the interface of the nondelaminated and delaminated regions (Ω_I) presented in matrix form as follows.

$$R\tilde{u} = 0 \tag{29}$$

where $\tilde{u}$, which is a subset of the **u**, contains the degrees of freedom in Ω_I and is partitioned as follows

$$\tilde{u} = \begin{bmatrix} u_{i=1} \\ u_{i=2} \\ u_{i=3} \end{bmatrix} \tag{30}$$

and $\mathbf{u}_i$ contains the nodal displacements in the i-th region (i.e. i = 1 refers to Ω as before) which are also contained in Ω_I as follows. A similar relationship is defined for $\ddot{u}$. The matrix R has the following form.

$$\mathbf{R} = \begin{bmatrix} \mathbf{R}_{i=2} & -\mathbf{I} & \mathbf{0} \\ \mathbf{R}_{i=3} & \mathbf{0} & -\mathbf{I} \end{bmatrix} \tag{31}$$

where the first column contains the submatrices $R_{i=3}$ and $R_{i=3}$ which in turn contain factors in terms of a_i, b_i and h. The exact formulation for these submatrices will be presented in the final paper. The Lagrangian for the discretized system is formulated as follows

$$L = \frac{1}{2}\left(\dot{\mathbf{u}}^T\mathbf{M}\dot{\mathbf{u}} - \mathbf{u}^T\mathbf{K}\mathbf{u} + \mathbf{u}^T\mathbf{F} + \mathbf{u}^T\mathbf{F}_p\right) + \frac{1}{2}p\left(\dot{\tilde{\mathbf{u}}}^T\mathbf{R}^T\mathbf{R}\dot{\tilde{\mathbf{u}}} + \tilde{\mathbf{u}}^T\mathbf{R}^T\mathbf{R}\tilde{\mathbf{u}}\right) \tag{32}$$

where the first four terms are the kinetic, strain and potential energies due to an applied load and piezoelectric actuation, respectively. The last two terms are penalty terms for the displacements and velocities multiplied by a penalty factor, p, to satisfy the continuity conditions at Ω_I. Differentiation of L with respect to the nodal degrees of freedom using the Lagrange technique allows the equations of motion to be reformulated to include the constraint terms while retaining symmetry. The resulting augmented equations are as follows.

$$[\mathbf{M} + p\mathbf{P}]\ddot{\mathbf{u}} + [\mathbf{K} + p\mathbf{P}]\mathbf{u} = \mathbf{F} + \mathbf{F}_p \tag{33}$$

where **P** is the penalty matrix defined as follows.

$$\mathbf{P} = \mathbf{R}^T\mathbf{R} \tag{34}$$

which is expanded to correspond to the global degrees of freedom (**u**).

Preliminary Results

Static response

Some numerical and experimental results are presented for a cantilever Gr/Ep composite plate with stacking sequence $[0°/90°/0°]_6$ and dimensions L = 25cm, W = 10cm, and h = 2.286mm. The thickness of each ply is 0.127mm which is typically used by industry. Plies numbered 13-16 are replaced with a single PZT piezoelectric layer of thickness 0.381mm which represents a commercially available piezoelectric material thickness. Material properties are presented in Table 1. The plate mesh has 25x10 elements and 2002 degress of freedom. The undeformed mesh with no delaminations is presented in Fig. 7. The piezoelectric layer is energized with a constant voltage of 150 volts. Both longitudinal bending and camber deflections are present due the actuation as

shown in Fig. 8. This is because the piezoelectric layer is offset from the neutral axis of the plate which produces bending moments about the X and Y axes. The finite element results correlate well with sample static experimental tests as shown in Fig. 9. In this figure, the transverse displacement is denoted (w*) and is normalized with respect to its maximum value. The lengthwise coordinate is denoted (x*) and is normalized to the length of the plate .

Next, the effects due to delamination are investigated using the above smart plate properties. Delamination is introduced at the interface between the composite substructure and the piezoelectric layer (plies 12 and 13) at the free end of the plate through the entire width (20 cm < x < 25 cm, 0 cm < y < 10 cm). The mesh for the composite substructure, located at the midplane of the nondelaminated portion of the plate, comprises 20x10 elements. Two additional 5x10 meshes are generated above and below the delamination at the midplanes of each respective region. These meshes are offset from the midplane of the undelaminated portion of the plate as shown in Fig. 10. It is important to note that Figs. 10 and 11 are not to scale so that the different meshes may be easily identified. Continuity at the interface of each of these delaminated regions and the composite substructure region is obtained by implementing the continuity conditions and penalty approach discussed earlier. The total number of degrees of freedom for the delaminated plate is 2541. Again, the piezoelectric layer is energized with a constant voltage of 150 volts. The static deflection in this case (Fig. 11) is significantly different from the first case (Fig. 8) where actuation produced bending which resulted in negative transverse displacements. The nondelaminated portion of the plate bends downward as before, as does the region below the delamination. However, the region above the delamination bends in a positive transverse direction. This is because the offset of the piezoelectric layer from the local midplane in the delaminated region is opposite the offset in the nondelaminated region. This results in a reversal of the bending moment due to the piezoelectric actuation and a positive transverse displacement. These preliminary results indicate that a thorough understanding of the effects due to delamination is critical to designing structures with smart composite materials. The final paper will present additional results to

investigate the effect of delamination on the static and dynamic response of a smart composite laminate.

Dynamic response

In this section, results are presented to demonstrate how the developed theory can be used to investigate issues related to active control and delamination. The test article is a composite cantilever plate with dimensions W = 5.08 cm, L = 45.72 cm, and thickness 1.16 mm. The material properties are again those of Gr/Ep (Table 1) and the stacking sequence is [0°/90°]4s. Two piezoelectric actuators with dimensions 2.54 cm (width) x 10.16 cm (length) x 0.762 mm (thickness) are bonded side by side on top of the laminate near the root of the plate as shown in Fig. 12. The actuators are linked electrically to function as a single unit. The piezoelectric sensors have the same width and height as the actuators. However, the thickness of the sensors is 0.381 mm. They are placed opposite the actuators on the bottom of the laminate and also function as a single unit. The first natural frequency of the laminate, which corresponds to the first bending mode, is ω_1 = 9.1887 Hz. A damping ratio of ξ_1 = 0.02 is assumed to represent the passive damping capability already present in the composite material. The laminate is initially loaded with a static distributed force of q = 30 kg/m^2 which is suddenly released at time t = 0. The sensor and actuator are coupled to a velocity feedback control loop which is designed to reduce vibratory amplitudes during the transient response as quickly as possible. Practical limitations dictate that the voltage supplied to the actuator must not exceed 100 volts. This corresponds to an electric field of 138 V/mm which is well below the maximum allowable electric field of the piezoelectric material. Five modes are included in the dynamic response analysis.

The test article is first examined with the control system turned off. The tip of the laminate is displaced 1 mm due the static load and is then released. The decay envelope due to passive damping alone is presented in Fig. 13. In this figure, the transverse displacement at the tip of the laminate (w) is presented for both the passive case and the active case which will be discussed shortly. The *1% settling time* (t_s), which is the time when the vibrational amplitude become 1% of the initial amplitude, is determined from the following equation.

$$t_s = -\frac{\log_e(0.01)}{\xi_1 \omega_1} \tag{34}$$

The 1% settling time for the passive damping case is found to be 3.732 seconds.

Next, the velocity feedback control system is turned on and the gain is selected to appropriately energize the actuators without exceeding the maximum allowable voltage. The voltage supplied to the actuators during the transient response is shown in Fig. 14 and does not exceed 100 volts. The active controls significantly increase the damping ratio of the composite laminate from 0.02 to 0.0513. This reduces the settling time by 61% to 1.455 seconds as shown in Fig. 15. The transient response for both passive and active cases are presented in Fig. 13 Thus, the piezoelectric sensor/actuator pair has a significant effect on increasing the damping of the laminate.

Now the effect of delamination on the control system is investigated. Delamination is introduced in the above test article at the tip of the actuator nearest the fixed end and extends throughout the width of the actuator at the interface of the bonded actuator and the composite substructure as shown in Fig. 16 The length of the delamination (L_d) is indicated by the nondimensional parameter β where $\beta = L_d/L$ and L is the length of the laminate. As the length of the delamination grows, the control authority is reduced since the actuator is less able to transfer the stresses, which are induced from the piezoelectric actuation, to the substructure. This reduction in control authority is indicated in Fig. 17 where the settling time is presented for a range of delamination lengths. The current model allows for both slipping and separation of delaminated layer (in this case the bonded actuator) from the composite substructure. Separation of the actuator at $\beta = 11\%$ is observed in the sixth mode, which is the fourth bending mode, at a frequency of $\omega_6 = 209.8$ Hz as shown in Fig 18. Separation of the delaminated actuator layer in one of the lower modes is unexpected and may significantly influence a more complex dynamic response, such as the case of a forced response.

Future work

Research plans that are either already under progress or are soon to be implemented are as follows.

- Complete mathematical investigation to study the use of smart materials for vibration control.
- Determine the effect of delamination on the authority of the control system.
- Develop and implement experimental procedure to validate proposed mathematical model.

References

1. Crawley, E. F. and Anderson, E. H. "Detailed Models of Piezoelectric Actuation of Beams" *Proc.* of the 30th AIAA/ASME/ASCE/AHS/ASC Structures, Structural Dynamics and Materials Conference, Mobile, Al., April 1989, pp. 2000-2010.

2. Lee C. K. "Theory of Laminated Piezoelectric Plates for the Design of Distributed Sensors/Actuators. Part 1: Governing Equations and Reciprocal Relationships" *Journal of the Acoustical Society of America*, Vol. 87, No. 3, March, 1990. pp. 1144-1158.

3. Chandrashekhara, K. and Agarwal, A. N. "Active Vibration control of Laminated Composite Plates Using Piezoelectric Devices: A Finite Element Approach" *Journal of Intelligent Material Systems and Structures*, Vol. 4, Oct. 1993, pp. 496-508.

4. Tzou, H. S. and Zhong, J. P. "Electromechanics and Vibrations of Piezoelectric Shell Distributed Systems" *Journal of Dynamic Systems, Measurement, and Control*, Vol. 115, Sept., 1993, pp. 506-517.

5. Robbins, D. H. and Reddy, J. N. (1991) "Analysis of Piezoelectrically Actuated Beams Using a Layerwise Displacement Theory" Computers and Structures, Vol. 41, No. 2, pp. 265-279.

6. Lee, H. J. and Saravanos, D. A. (1995) "Coupled Layerwise Analysis of Thermopiezoelectric Smart Composte Beams" AIAA Journal, Aug., submitted for possible publication.

7. Mitchell, J. A. and Reddy, J. N., "A Refined Hybrid Plate Theory for Composite Laminates with Piezoelectric Laminae", *International Journal of Solids and Structures*, Dec. 1994, Vol. 00, No. 0, pp 1-24.

8. Reddy, J. N. "A General Non-Linear Third-Order Theory of Plates with Moderate Thickness" *International Journal of Non-Linear Mechanics*, Vol. 25, No. 6, 1990, pp. 677-686.

9. Chattopadhyay, A. and Seeley, C. E. "A Higher Order Theory for Modeling Composite Laminates with Induced Strain Actuators" *Composites Part B: Engineering*, Feb. 1996, *accepted for publication.*

10. Yang, H. T. Y. and He, C. C., "Three-Dimensional Finite Element Analysis of Free Edge Stresses and Delamination of Composite Laminates", *Journal of Composite Materials*, Vol. 28, No. 15, 1994, pp. 1394-1412.

11. Whitcomb, J. D., "Three Dimensional Analysis of a Postbuckled Embedded Delamination", *Journal of Composite Materials*, Vol. 23, 1989, pp. 862-889.

12. Pavier, M. J. and Clarke, M. P., "A Specialized Composite Plate Element for Problems of Delamination Buckling and Growth" *Composite Structures*, Vol. 35, 1996, 45-53.

13. Whitcomb, J. D., "Finite Element Analysis of Instability Related Delamination Growth" *Journal of Composite Materials*, Vol. 15, 1981, pp. 403-426, ,

14. Kardomateas, G. A and Schmueser, "Buckling and Postbuckling of Delaminated Composites Under Compressive Loads Including Transverse Shear Effects", AIAA Journal, Vol. 26, No. 3, 1988, pp. 337-343.

15. Gummadi, L. N. B. and Hanagud, S. (1995) "Vibration Characteristics of Beams with Multiple Delaminations" *Proc.* 36th AIAA/ASME/ASCE/AHS/ASC Structures, Structural Dynamics and Materials Conference - Adaptive Structures Forum, New Orleans, LA, Apr. 10-14, pp. 140-150.

16. Barbero, E. J. and Reddy, J. N., "Modeling of Delamination in Composite Laminates Using a Layer-wise Plate Theory" International Journal of Solids and Structures, Vol. 28, No. 3, 1991, pp. 373-388.

17. Chattopadhyay, A. and Gu, H. "A New Higher-Order Plate Theory in Modeling Delamination Buckling of Composite Laminates" *AIAA Journal*, Vol. 32, No. 8, 1994, Aug., pp. 1709-1718.

18. Chattopadhyay, A. and Gu, H. "Elasticity Solution for Delamination Buckling of Composite Plates", *Proc.* 37th AIAA/ASME/ASCE/AHS/ASC Structures, Structural Dynamics and Materials Conference, Salt Lake City, UT, Apr. 15-18. 1996.

19. Wang, J. and Lin, C., "Vibration of Beam-Plates Having Multiple Delaminations", *Proc.* 36th AIAA/ASME/ASCE/AHS/ASC Structures, Structural Dynamics and Materials Conference - Adaptive Structures Forum, New Orleans, LA, Apr. 10-14, 1995.

20. Seeley, C. E. and Chattopadhyay, A. "Modeling Delaminations in Smart Composite Laminates" *Proc.* of the 37th AIAA/ASME/ASCE/AHS/ASC Structures, Structural Dynamics and Materials Conference and Adaptive Structures Forum, Salt Lake City, UT, Apr. 15-19, 1996, pp. 109-119.

Table 1. Material properties.

	Gr/Ep	PZT
E_1 (GPa)	143	63.0
E_2 (GPa)	9.70	63.0
ν_{12}	0.300	0.300
G_{12}, G_{13} (GPa)	6.00	24.2
G_{23} (GPa)	2.50	24.2
ρ ($x10^3$ Kg/m^3)	1.39	7.60
d_{31} ($x10^{-12}$ m/V)	-	253

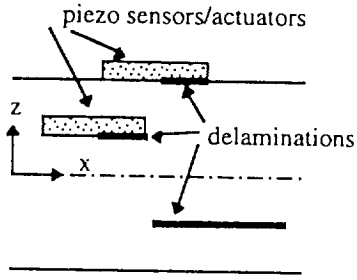

Figure 1 Composite laminate cross section.

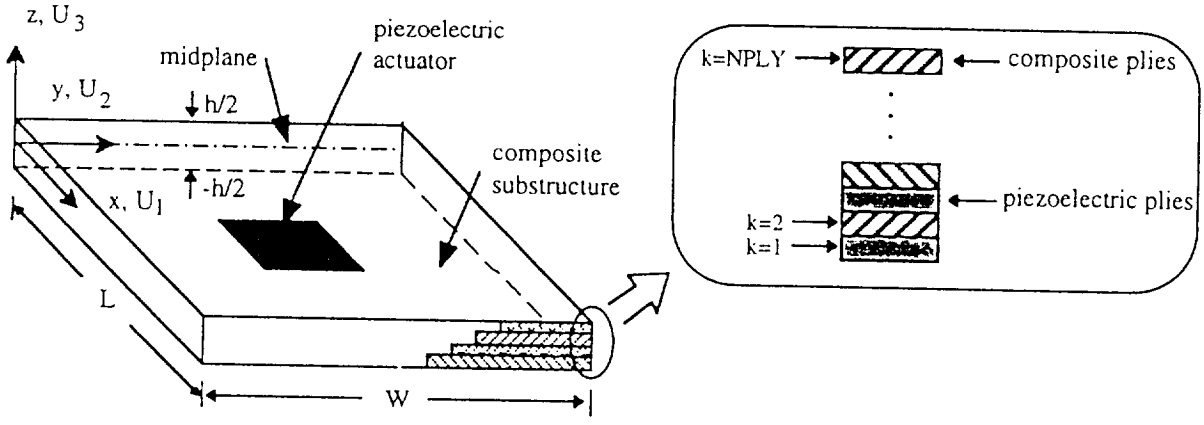

Figure 2 Smart composite plate incorporating piezoelectric layers.

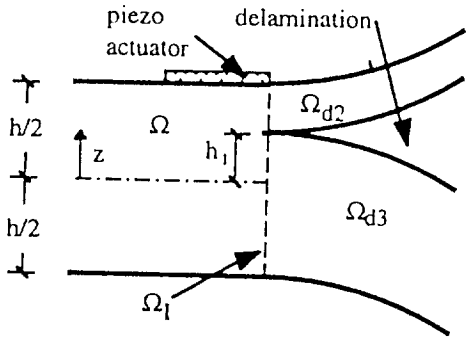

Figure 3 Laminate cross section.

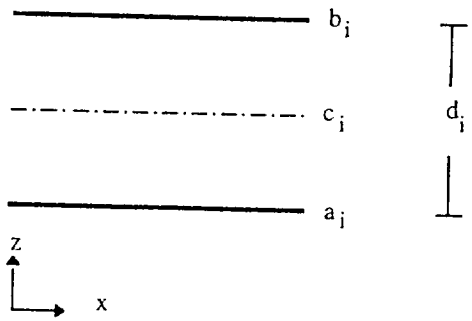

Figure 4 Local region plate geometry.

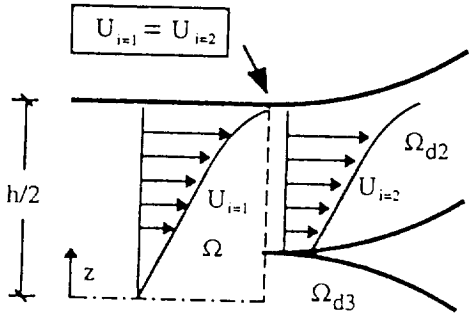

Figure 5 Displacements in cross section.

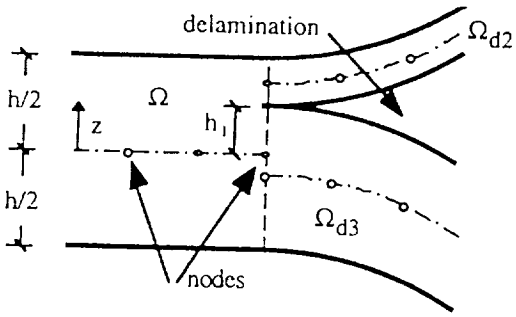

Figure 6 Finite element discretization.

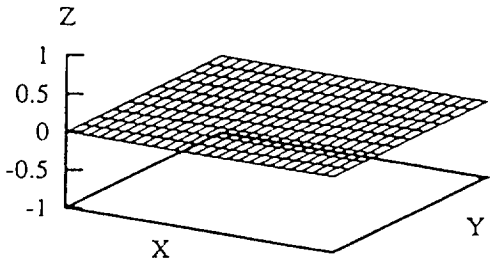

Figure 7 Undeformed plate mesh.

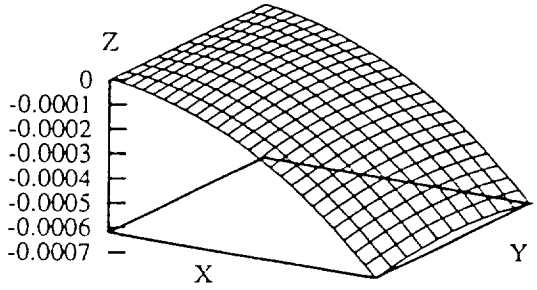

Figure 8 Static deflection due to piezo actuation.

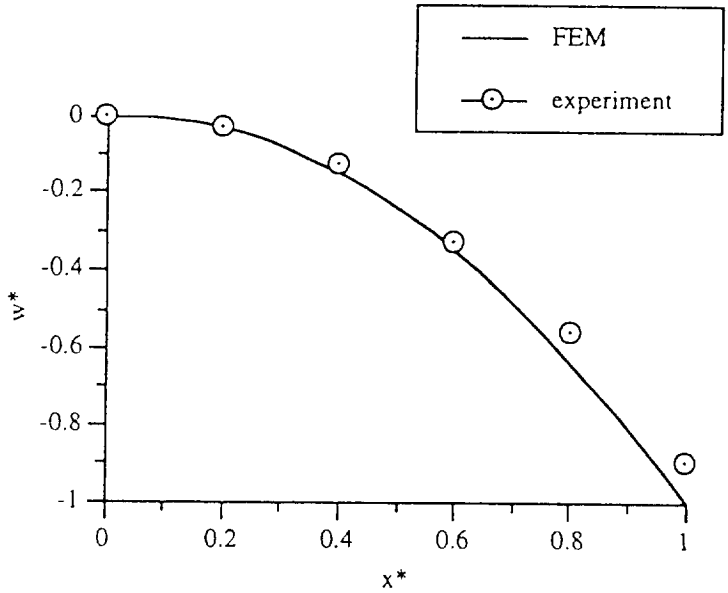

Figure 9 Normalized static displacement FEM and experimental results.

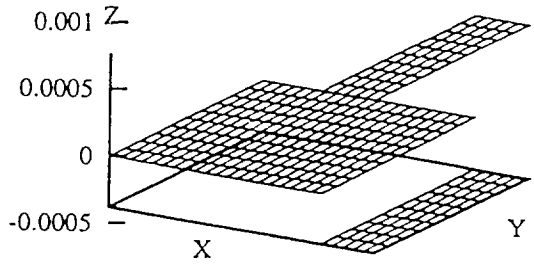

Figure 10 Undeformed mesh including delamination.

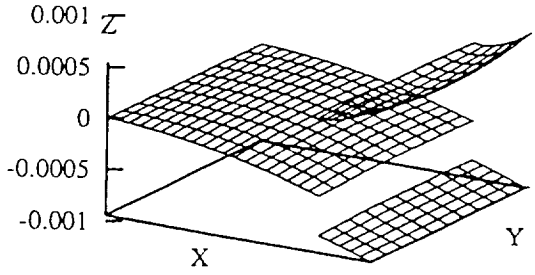

Figure 11 Static deflection due to piezo actuation including delamination.

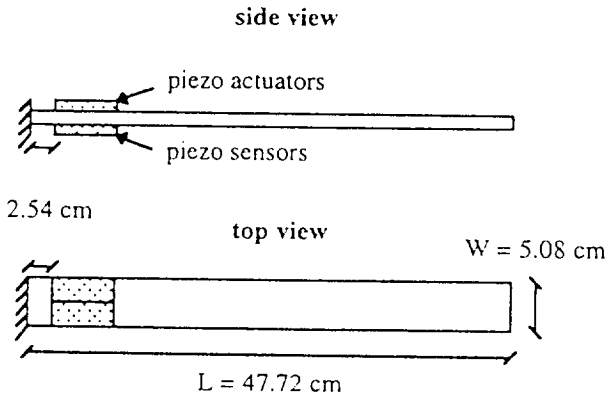

Figure 12 Gr/Ep laminate with bonded piezo sensors/actuators.

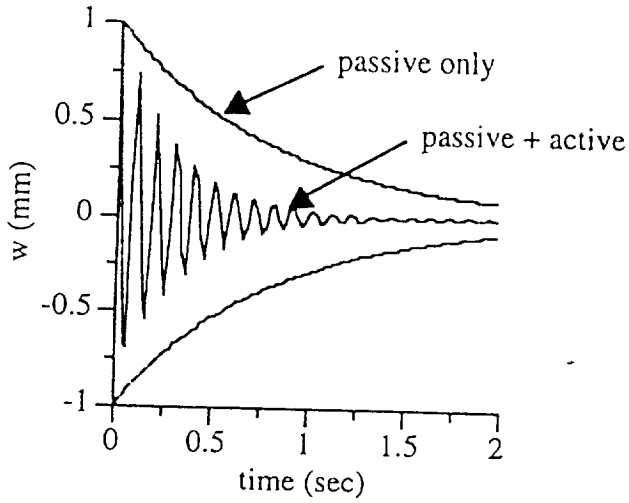

Figure 13 Passive / active transient response.

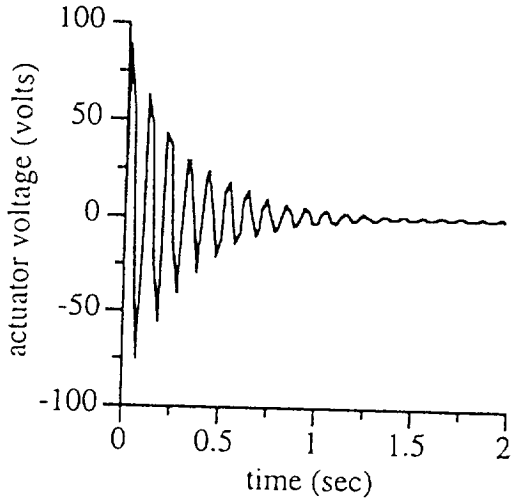

Figure 14 Actuator voltage.

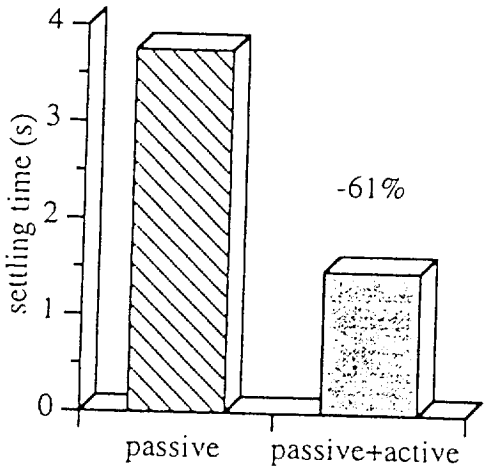

Figure 15 Decrease in settling time due to active control.

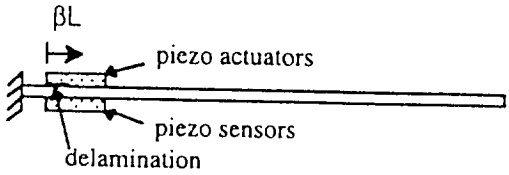

Figure 16 Composite laminate with delaminated actuators.

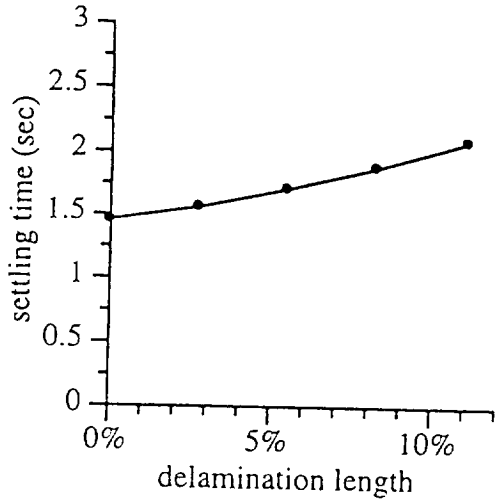

Figure 17 Increase in settling time due to delamination.

Z

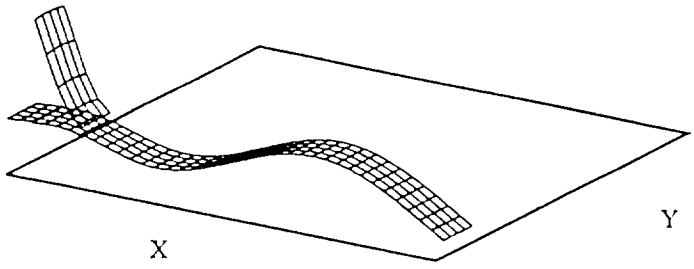

Figure 18 Separation of delaminated layer in mode 6.